BRNO UNIVERSITY OF TECHNOLOGY

VYSOKÉ UČENÍ TECHNICKÉ V BRNĚ

FACULTY OF MECHANICAL ENGINEERING

FAKULTA STROJNÍHO INŽENÝRSTVÍ

INSTITUTE OF SOLID MECHANICS, MECHATRONICS AND BIOMECHANICS

ÚSTAV MECHANIKY TĚLES, MECHATRONIKY A BIOMECHANIKY

ANALYSIS OF METHODS OF MODELING BONE LOSS DUE TO OSTEOPOROSIS

ANALÝZA ZPŮSOBŮ MODELOVÁNÍ ÚBYTKU KOSTNÍ HMOTY VLIVEM OSTEOPORÓZY

BACHELOR'S THESIS

BAKALÁŘSKÁ PRÁCE

AUTHOR   Lucie Orlová

AUTOR PRÁCE

SUPERVISOR   Ing. Petr Vosynek, Ph.D.

VEDOUCÍ PRÁCE

BRNO 2019

Bachelor's Thesis Assignment

Institut:	Institute of Solid Mechanics, Mechatronics and Biomechanics
Student:	**Lucie Orlová**
Degree programm:	Engineering
Branch:	Fundamentals of Mechanical Engineering
Supervisor:	**Ing. Petr Vosynek, Ph.D.**
Academic year:	2018/19

As provided for by the Act No. 111/98 Coll. on higher education institutions and the BUT Study and Examination Regulations, the director of the Institute hereby assigns the following topic of Bachelor's Thesis:

Analysis of methods of modeling bone loss due to osteoporosis

Brief description:

The subject of the thesis is a research study of methods of bone tissue modeling at different levels of geometry and ways of simulating bone loss at these different levels. The obtained information will be then used to create computational models of bone tissue at the micro level. The stiffness or another appropriate parameter will be analyzed.

Bachelor's Thesis goals:

- a literature review of bone tissue modeling types
- creation of computational models according to the previous point
- models comparison

Recommended bibliography:

DE, Suvranu, Farshid GUILAK a Mohammad R. K. MOFRAD. Computational modeling in biomechanics. New York: Springer, c2010. ISBN 978-90-481-3574-5.

VOSYNEK, P. Analýza odezvových veličin kostní tkáně při mechanickém zatěžování. Brno: Vysoké učení technické v Brně, Fakulta strojního inženýrství, 2015. 98 s. Vedoucí dizertační práce Ing. Tomáš Návrat, Ph.D.

Students are required to submit the thesis within the deadlines stated in the schedule of the academic year 2018/19.

In Brno, 29. 10. 2018

L. S.

_____

_____

prof. Ing. Jindřich Petruška, CSc.
Director of the Institute

doc. Ing. Jaroslav Katolický, Ph.D.
FME dean

Summary

This Bachelor's Thesis introduces the topic of bone biomechanics. The main aim of the paper is to research solutions for computational modeling of the structure of long bones. Furthermore, the osteoporotic changes to this structure are described. Along with the research, some basic biological terms and mechanical principles are introduced. Based on the information gathered in the theoretical part of the work, finite element method computations are performed in ANSYS software.

Abstrakt

Tato bakalářská práce se zabývá biomechanikou kosti. Hlavním cílem je teoretický průzkum řešení pro výpočtové modelování dlouhých kostí a změn této struktury vlivem osteoporózy. V rámci rešerše jsou vysvětleny související biologické pojmy a základní principy mechaniky. Na základě informací shromážděných v teoretické části práce jsou provedeny výpočty pomocí metody konečných prvků v programu ANSYS.

Keywords

Computational modeling, bone model, biomechanics of the bone, osteoporosis, ANSYS.

Klíčová slova

Výpočtové modelování, model kosti, biomechanika kosti, osteoporóza, ANSYS.

Rozšířený abstrakt

Hlavním cílem této bakalářské práce je vytvoření teoretické rešerše způsobů výpočtového modelování struktury dlouhých kostí na různých úrovních geometrie a jejích teoretických či náhradních modelů. Do přehledu jsou zahrnuty a okomentovány způsoby modelování kompaktní a spongiózní kosti s důrazem na komplexitu mikrostruktury trámčité kostní tkáně a variabilitu způsobů nahrazování této struktury (například náhrada pruty nebo kombinace prutové a destičkové náhrady).

Rešerše teoretických modelů je posléze doplněna o souhrn základních mechanických vlastností kostní tkáně jako jsou například hustota, elastický (Youngův) modul a tuhost, které jsou využívány k výpočtovému modelování chování tkáně pod zatížením a odvození dalších charakteristik. V rešerši je také zahrnuta klasifikace tohoto biomateriálu mezi ortotropní skupinu, avšak materiál pro další analýzu je v zadání práce definován jako izotropní. Rozdíl mezi těmito dvěma modely není zanedbatelný co se týče celkové analýzy vlastností tkáně, avšak při tlakovém či tahovém zatěžování jsou elastické moduly v hlavním směru (směr běžného zatěžování) srovnatelné.

V návaznosti na předchozí shrnutí jsou okomentovány změny makro- a mikrostruktury kostní tkáně pod vlivem osteoporózy, což je degenerační nemoc postihující kostní tkáň, známá také pod názvem řídnutí kostí. Je způsobena nadměrnou resorpcí tkáně, což způsobuje úbytek kostní hmoty a zvyšování porozity povrchu. Osteoporóza mění nejenom geometrickou strukturu, ale také již zmiňované mechanické vlastnosti, zejména tuhost, a tím i schopnost kosti odolávat nárazům.

Na základě informací shromážděných v teoretické části práce je proveden výpočet jedné ze základních mechanických veličin: elastického modulu na základě CT snímků ženské holenní kosti z kolekce Visible Human. Výpočet elastického modulu je založen na vizualizaci geometrie kosti pomocí programu ITK-SNAP, samotný výpočet modulu je následně proveden v nástroji Bonemat, ve kterém je dle odstínu zobrazení přiřazována hodnota hustoty, na jejímž základě je proveden samotný výpočet.

Analýza kompaktní kosti je zaměřena zejména na makroskopické hledisko, vzhledem k tomu, že je samotná tkáň idealizována jako neporózní materiál. K tomuto účelu je výpočtově odvozena geometrie diafýzy holenní kosti, která je posléze analyzována metodou konečných prvků (MKP) v programu ANSYS Workbench 19.2 při namáhání převážně tlakovém, čímž se simuluje zatížení kosti při stání. Pro určení změny chování diafýzy ovlivněné osteoporózou, je geometrie diafýzy následně idealizována jako prut mezikruhového průřezu tak, aby odpovídala geometrii a deformaci reálné struktury. Následně je šířka vrstvy kompaktní kosti přizpůsobena hodnotám osteoporotické tkáně a podrobena kompresi.

Další odvozenou reprezentací geometrie jsou modely malých objemů trámčité kosti, které jsou posléze podrobeny idealizaci dle předchozí rešerše, a to pomocí prutů různého průřezu a destičkového modelu. Geometrie spongiózní tkáně byla odvozena z CT snímků lidské lebky, jelikož CT snímky holenní kosti nejsou vhodné pro makroskopickou analýzu, zejména kvůli k nízkému rozlišení těchto snímků, ze kterých model trámčité kosti vzešel jako plný materiál. Jak výpočtově odvozený model, tak i jeho idealizovaná reprezentace jsou podrobeny kompresi a výsledný posuv je porovnán.

Závěrečná část bakalářské práce je věnována osteoporotickým změnám, které jsou dle údajů z rešeršní části aplikovány na vytvořené teoretické modely. U idealizovaného modelu kompaktní kosti je snížena tloušťka vrstvy a takto modifikovaná geometrie je

opět podrobena analýze. S ohledem na předchozí rešerši není žádný jiný typ transformace aplikován.

Idealizovaný model trámčité kosti je podroben dvojí transformaci: geometrické transformaci a transformaci mechanických vlastností, a to snížením elastického modulu tkáně. Geometrická transformace je na základě předchozího výzkumu provedena odebráním prutů ze soustavy, což simuluje úbytek propojení, a navíc jsou sníženy rozměry těchto prutů. Výsledná deformace jednotlivých vygenerovaných reprezentací je porovnána a náležitě vyhodnocena.

I declare that I have written the Bachelor's thesis *Analysis of methods of modeling bone loss due to osteoporosis* on my own and under the guidance of my Bachelor's thesis supervisor Ing. Petr Vosynek, Ph.D., and using the sources listed in references.

Lucie Orlová

Contents

1. Introduction

Biomechanics is the scientific field of study which applies engineering principles into biological systems. In other words, apart from understanding the physiology of the subject, it is crucial to understand basic mechanical principles. This knowledge helps us not only to comprehend how biological systems work but also to visualize the inner structure of each part of the system.

The complexity of the biomechanical problems is based mainly on the demanding character of representing the geometry of the biomaterials, such as muscles, soft tissues, and bones. Following the knowledge gained by visualizing the biological structure thoroughly and understanding its value, it is possible to determine potentially dangerous factors and possibly predict or even prevent them.

Visualization of such a complex structure as cancellous, muscular or neural tissue would not be possible if the computational tools did not exist. The computational models of the living tissues are simplifications of the real materials created by omitting negligible variables. In the case of bone modeling - at least for the present time, the accuracy has become sufficient for further analysis. The required accuracy for the models is accomplished by establishing the models based on data obtained either using *in vivo* scanning methods, for example, computed tomography or X-ray methods, or by *in vitro* experiments, that are performed outside of the living organisms, for example, three-point bending.

The main subject of this study is the skeletal system of the human body, which serves as the main support for other tissues. This system consists of more than two hundred bones and the connections between them. The system not only provides support for the body but also enables movement and protects the soft tissues. Since the microstructure of the bone forms as a reaction to the loading conditions and every bone withstands different loading conditions, the variety of microstructure arrangement is wide.

2. Theoretical part

The human skeletal system can be defined as *an internal support structure formed by bones and connective tissue*, such as joints [3]. The functions of the two parts differ with the characteristics of each. The subject of this thesis, the bones, form the rigid frame responsible for the strength and shape of the human body.

Apart from the structural function bones also behave as a functional tissue, ensuring storage place for calcium. Calcium is a valuable part of the human system, for example, it enables the nerve conduction.

The system is composed of a complex system of lamellas [1] that provide the bone with the unique capability to adapt to increased physical activity or a fracture, however, the process of adaptation has not yet been fully described. Generally, the tissue reacts to those impulses by changing the inner structure to redirect potentially critical loads, e.g. altering structural orientation [15] and therefore replacing bending moment with less demanding loads, compression or tension [1]. It is achieved by redirecting the bending moment either in the inner structure, by altering the density and rebuilding the structure for long-term loads [15] or with the help of muscles in an impact load. The replacement is necessary since the material shows higher ultimate tensile strength in comparison with the ultimate shear strength [1], which is up to three times lower. This concludes, that the bones are more resilient to tensile and compression loading than to any other type of loading.

The overall shape of the bones differs with respect to their function and location in the body, the most common distribution is by the shape: long, short and flat bones [2].

The long bones of the leg, such as femur or tibia, were chosen as a main subject for the thesis since those bones tend to withstand the greatest loads in the skeletal system because they carry all of the body weight. The long bones found in the arm, e. g. humerus, ulna or radius could also be used for the analysis, thanks to the similar distribution of different morphological types of the tissue and their overall shape, however, bones in arms are usually exposed to minor loading.

The body of long bones can be divided into two parts: a cylindrical shaft called diaphysis [3] and a wider rounded end on each side, the epiphysis. The connection between them is called metaphysis, which contains the growth plate allowing the bone to grow in length during the first years of the human body development. After the end of the growth stage, the epiphysis and metaphysis fuse.

2.1. Bone tissue

The most suitable way to describe the bone tissue is using the cross-sections of the epiphysis of the femur, tibia or humerus. The tibia or the shinbone was also chosen as the main subject of this paper, because of its properties such as bone tissue distribution and loading factor are most convenient for the research. The numerical evaluation of the key properties will be further described in section 4.3.

2.1.1. Bone material composition

The material of bones can be described as a composite material with small density and excellent strength and stiffness, which is constantly rebuilding and self-repairing [5].

Roughly a third of the dry bone mass composition is occupied by bone matrix, the other two-thirds are formed by the bone mineral. The bone within the living organism usually contains about 10 to 20 percent water [6]. The composition of the matrix is as follows: collagen fibers, proteins, and inorganic mineral, especially hydroxyapatite [3].

Collagen forms a triple helical structure and specific points serve as a deposit site for the mineral crystals. The mineral, which is approximately 225nm long and 10nm thick [3], can be found between the fibers as well as inside of them [6].

As a result of the fact that the composite structure is not uniform [4], symmetrical, isotropic, linear or homogenous, the diverse mechanical properties appear locally [3] (for example in spongy, mechanical properties vary significantly even within one metaphysis [15]). The imperfections of the bone structure can be divided into two groups: the heterogeneity of the material itself - tissue heterogeneity [2] and differences in the overall structure - structural heterogeneity [7]. These irregularities reduce the reliability of the FE analysis (even for medical purposes), also because they are not yet fully described [8], especially when it comes to the tissue heterogeneity.

It is important not to underestimate the impact of heterogeneity on tissue properties in the following research, yet the models, that to be generated in this thesis will be considered homogeneous, even though it will induce some minor errors. Those errors will surely impact the analysis, although the estimated properties should correspond to the real properties 3.

Bone modeling and remodeling

After the initial process of woven bone being ossified and forming lamellar bone, all types of bone start to remodel and reconstruct [3]. The process of bone remodeling is continuous and its main purpose is to adapt to the changes of mechanical loads, replace the old tissue or replace the tissue damaged by cyclic loading. [9] The bone development and remodeling consist of two processes: new bone formation (*ossification*) that prevails over the disassembly of the old tissue (*resorption*), see table 2.1 [3, 6]. Sometimes, the literature as Cowin's Bone Mechanics Handbook also mentions the quiescent state that occurs at 96,6% of the cortical bone surfaces and 92,8% of cancellous bone surfaces highlighting the fact, that bone cells do not act on all bone surfaces at once [3].

The total turnover can differ with hormonal activity. In fact, hormones play important part of bone growth as well [3].

There exist three types of cells, that are necessary for proper growth and development of bones: osteoblasts, osteocytes, and osteoclasts [2]. The osteoclast is a huge bone resorbing cell [3], that breaks down the old tissue, creating a space for osteoblasts, a cuboid bone-forming cells. Osteoblasts then create a cement line and lamellar bone. The third type of bone cells are osteocytes, which are in fact osteoblasts trapped inside the bone during the remodeling of the tissue.

Table 2.1: Modeling and remodeling characteristics according to source [3].

Parameter	Cortical	Cancellous
Forming	3,0%	6,0%
	124 days	91 days
Resorbing	0,6%	1,2%
	24 days	21 days
Quiescent	96,6%	92,8%
Total remodeling time	148 days	112 days

2.1.2. Bone type classification

Two main morphological types of the tissue can be distinguished in all bones: cancellous and cortical bone. The main differences are in the density, structure, porosity, etc. Whereas the cortical bone forms 80% of the total skeletal mass, it only occupies 33% of the total bone surface [3].

Another type of bone tissue, present only at a newborn body or at healing fractures, is the woven bone which ossifies at the age 24 to 36 months of life [3] transforms to a lamellar bone. The formation of the woven tissue is usually a lot faster than the formation of lamellar bone and occurs in case of an emergency. This structure has one great disadvantage though, its stiffness is way lower than the stiffness of the lamellar bone. The reason is probably the haphazard structure of the bone as well as the lower mineral content.

The cartilage also plays a significant role in the case of bone growth. This type of tissue covers the joints and is mainly composed of water (forming 60% of the total cartilage mass) [10]. Nor the cartilage nor the woven bone are the main concern of this thesis, therefore, they will not be discussed any further.

Bone marrow is filling the spaces between the lamellae of the porous tissue in the cancellous bone as well as the bone cavities [2]. Two types of tissue can be distinguished: red and yellow. The red bone marrow is responsible for blood cell production and changes to the yellow inactive marrow with age.

Cortical bone

The compact or cortical bone can be described as a dense outer envelope of the bone [3]. At long bones, it forms a cylinder that surrounds the bone marrow at the shaft and an outer thin shell at joints.

At a micro level, the cortical bone is characterized as a lamellar bone [3]. The structure is formed by relatively small rod-shaped units called osteons, that have very good mechanical strength, given by their configuration in the direction of principal stresses.

Osteons can be simplified as basic cylindrical units with a diameter between 100 and 300 micrometers with a center formed by a Haversian canal, that serves as a transport canal for blood. Osteons further consist of concentric lamellas that are 1 to 5 micrometers thick (about the same thickness as the spongy rods), see figure 2.1, further composed of collagen fibers, that have the same direction within one layer, however different orientation between layers of lamellae. This type of lamellar structure together forms a 0,5 to 2 mm thick layer on the surface of the bone, which along with higher density and lower

porosity contributes to higher strength, elastic modulus, and other mechanical properties in comparison with spongy structure.
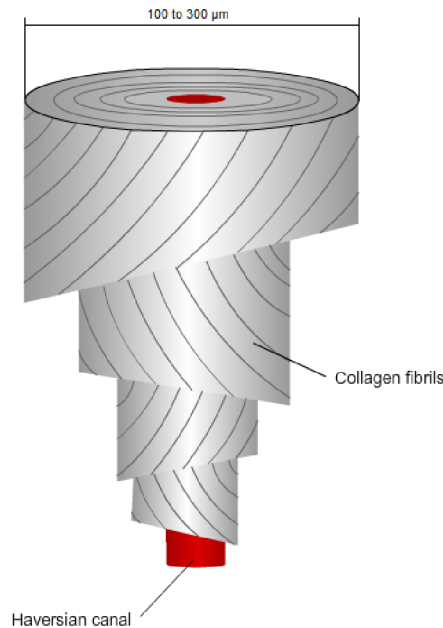

Figure 2.1: Schematic representation of an osteon, the basic unit of a cortical bone.

Cancellous bone

While cortical bone is composed of concentrated rod structure, the cancellous bone, spongy or trabecular bone consists of a rods-and-plates system. Cancellous bone is therefore often described as *composite, anisotropic, open porous cellular solid* [7], in other words, its structure is open and honeycomb-like [6]. It is the inner filling of the mature bone, that is light and not dense [8], therefore it provides maximum strength for a minimum mass of the skeletal system [11].

Altogether, it can be assumed, that the orientation of the net formed by rods and plates (and transitions between them) follows the direction of the highest principal stresses [2, 3].

2.2. Osteoporosis

As a result of the medicine advancing rapidly, the life expectancy has increased [10] in the last decades, new age-related problems have been introduced. Osteoporosis, which is *the loss or dysfunction of skeletal tissue*, can be considered one of them even though age is not the only reason for its development. During the increasing years, as the bone micro- and nanostructure is continuously remodeled [15], the unbalanced rate between formation and resorption can occur. Generally speaking, the resorption starts to prevail at the age of 30 or 40 [1], which means that the bone loses its volume. At roughly 23% of the world population, the speed of the bone loss is out of the ordinary and subsequently comes with unpleasant symptoms, therefore it is spoken of as osteoporosis. In the early stage of osteoporosis, excessive resorption affects mainly cancellous bone [15] because of the high surface to volume ratio and porosity [4] of this type of tissue. However more

dire state occurs, when the increased resorption reaches the cortical bone, which becomes more porous causing the surface for remodeling increase even further, which also increases the speed of the resorption. Figure 2.2 maps the resorption of bone tissue affected by the age of subjects.
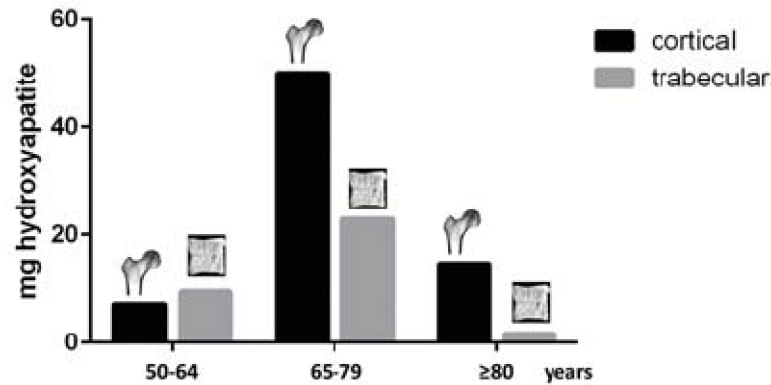

Figure 2.2: Bone loss affecting trabecular and cortical bone through mid to late stage of osteoporosis. Adapted from [15].

According to research [11], women are more likely to suffer from osteoporosis, because their bones are in average 23% smaller than men's at the same age. Moreover, some parts of the bones are weaker than the other. This results in fractures at the neck of the femur occurring in women with osteoporosis, 65 or more years old, being the most common type of fractures [8]. This does not mean there are no exceptions for those statistics, genealogy also plays a significant role.

The state of bones affected by the bone tissue loss are considered very dangerous for the patient, therefore, the aim of the bone tissue engineering is to prevent its most serious symptom: osteoporotic fractures. Some advanced X-ray scans have been developed to measure the Bone Mineral Density (BDM). Comparing the measured value with a standardized number leads to a conclusion, whether the patient is at risk or not [12].

2.2.1. Development of the osteoporosis

Following the former information, the age of 50 is the point at which the first, after which the first symptoms of the disease appear [12], even though the resorption prevails from the age of 30 2.2. As stated before, age is not the only factor playing a crucial role in the development, trauma, injury or even lifestyle choices can trigger the imbalance earlier.

Osteoporosis changes the structure, density or the composition of the bone [5]. To have an idea about the rate of density changes affecting both cancellous and spongy tissue, the average bone mass density loss is approximately 5% per ten years in women, whereas only 2,5% per decade in men [11]. Those results were obtained using the most accurate method - a long-term study, that was carried out at a large scale for example by Riggs et al. with more than a thousand individuals. It is possible, that in this case, most of the outstanding individuals (for example with diverse loading history) did not affect the result by more than 0,001%.

Another important fact is to mention the significance of the decreasing diameter of the bone [11] as a whole, which is also a result of skeletal aging. Since the overall stiffness, strength and other important mechanical properties are dependent on the cross-section, they also decrease with progressing osteoporosis. Additionally, porosity caused by prevailing resorption of the cancellous bone is linked with decreasing elastic modulus and yield stress [15], as the size of the pores increases (e. g. causing values of strength decrease locally), which affects the probability of propagation of microcracks.

As for the effects of osteoporosis on the micro level, the most noticeable effect of the prevailing resorption is found at the cancellous tissue [3], since this type is already less dense in its natural form and it is a subject to higher turnover 2.1. The geometry of the cancellous bone is affected in a manner, that can be observed on micro-CT scans easily. As a side effect of decreasing volume, some of the connections between plates are lost [1] and not replaced by new ones, the rest are affected by decreasing their diameter.

The osteoporosis can develop small pores on the surface of the cancellous bone, but the most noticeable effect is the diminishing cortical layer thickness. The research [26] conducted on a large scale in India, had determined the average difference in cortical thickness being 0.152 mm (between subjects younger than 50 years and a group of people older than 70 years of age).

According to all the knowledge summarized above, the geometric properties chosen as the main focus during the analysis of osteoporotic changes cross-sectional area of the bone (more specifically the cortical layer thickness), but mainly the deformation of the tissue under loading.

2.2.2. Engineering solutions

The current way of solving bone tissue loss is to replace or restore the damaged tissue. One of the possibilities to approach the bone tissue loss is either by total replacement of the diseased parts, e. g. hip joint replacement [10], or replacement of the tissue and renew the normal biological behavior. It is important to mention that the second approach is not yet optimal due to the side effects indicated in some cases[8].

There are four ideas on the biomaterials, that are currently being engineered to help the tissue regenerate and restore the functioning biology: bioceramics, natural polymers, synthetic polymers and hydrogels [8]. Current research is focused on the delivery of those materials through injection and fabrication of implants by additive technologies (3D printing)

3. Models of the bone

As mentioned before, long bones are usually the most suitable subject for the study of the bone structure due to their shape and structural diversity. Both cancellous and compact bone can be observed at the tibia, especially interesting area is found at its joints. The tubular shaft is formed mostly by rigid cancellous bone. Another reason for the choice is that when those bones are affected by osteoporosis, the density and structure changes are easier to distinguish.

To make a satisfying representation of the bone geometry, the computational tools combined with medical imaging tools need to be used. With the decreasing volume of the smallest element, the quality of the obtained geometry increases. The CT scans can be used for modeling the whole bone, even though it is impossible to extract the data for deriving the microstructure model. Micro-CT scans and micro-MRI scans are the most suitable medical imaging methods for this type of problem so far.

For purposes of this thesis, the constitutive bone material will be considered isotropic, homogeneous linear elastic continuum, which is sufficient for describing the tissue behavior at small strains [4]. By exceeding the limit value of only around 0,4% of apparent strain, this constitutive model becomes highly inaccurate and needs to be replaced by the nonlinear model.

3.1. Overview of solutions

The most models are based on the data extracted from the medical images [12] (CT, MRI, etc.) in combination with a 3D finite element method. Seemingly more basic models are focused on the whole-bone level, determining mechanical properties based on the geometry and loads. The results of macrostructure analysis provide default information for further modeling the bone structure at a micro level. This section will be focused mainly on the overview of existing theoretical models of the microstructure (with idealized geometry), the subsequent FE method application to those models will be further discussed in chapter 4.

The main benefit of the idealized tissue geometry is the fact, that together with accurately assigned material properties, it can be easily manipulated [4] e. g. to simulate osteoporotic changes. On the other hand, the replacement of the bone geometry sometimes induces extreme values at the element boundaries, which requires correction by smoothing algorithms. The more accurate the model is, the more complex equations and algorithms need to be used, which increases the costs of the method.

The idealization of the geometry is therefore achieved by replacing the real elements - obtained by medical imaging methods - by less complex structures [3] as plates, beams, solid elements, shells or a combination of those [4].

3.2. Cortical bone model

Although compact bone is not a homogeneous material, it is often considered to be, since it consists of a very similar arrangement of osteons (as mentioned above) and the space between the full osteons is filled with osteon-like structure [3] called interstitial osteon, a remaining part of a remodeled osteon. Therefore, it is often modeled as an undivided

layer on the surface of the bone. The shape of the cortical bone layer can be divided into two base shapes, a hollow beam at the shaft and a thin shell at the joint [1].

Compared to the wide variety of conducted research referring to the spongy tissue, there exist only little sources, that analyze the heterogeneity of the structure in more detail. An example of a more complex analysis of the cortical geometry [20] is represented by a homogeneous beam (see the picture 3.1 with cylindrical void spaces, which simulates the stress concentration factor of Haversian channels present in the center of an osteon, yet other irregularities such as interstitial osteons or anisotropy are not included in the analysis.
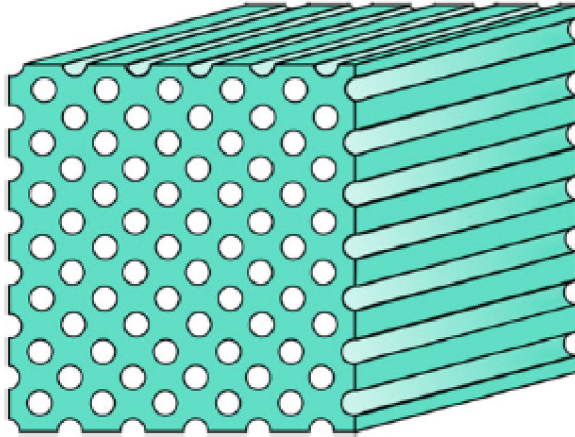

Figure 3.1: Idealized geometry of cortical bone [20].

3.3. Cancellous bone model

Mapping the cancellous bone structure and its properties is far more challenging due to small dimensions of plates and connections between them. Thanks to the computed tomography and X-ray scans that can collect images at a resolution up to 10 microns [11], it is possible to study elements of the cancellous bone at least visually. The most suitable imaging method for this task is micro-CT scan with a resolution of 100 micrometers [3] to distinguish between different types of tissue or even smaller to distinguish gaps and tissue. As for direct measuring of spongy tissue properties, it has proven ineffective and unreliable, as it was almost impossible to extract samples from test subjects - the most common are mice [4]. Even though the computational approach is prevailing nowadays, combining it with the experimental measurements brings even more accurate results, which is beneficial especially in the research area.

To illustrate the dimensions of the cancellous bone, the diameter of the connections between plates in the spongy structure has been estimated between 1 to 4 micrometers based on the lamellar thickness [3]. The porosity of the material ranges from 70% to 90% [4]. Even though simple units such as beams are representing the cancellous bone, the structure itself is still too complex for manual establishing - especially for modeling larger volumes.

3.3.1. Beam models

The models created only by the use of connected beam units, for example, in source [4], are a very accurate substitute, especially with the assistance of automatic geometry recognition software, that adjust the elements (their dimensions and orientation) to preserve the shear and bending deformations of the real tissue. The beam unit needs to be designed according to the beam theory in order to transfer loads and respond to the loading condition in a similar way as the real structure.

The computational approach to generating the haphazard beam geometry of the spongy is using the Voronoi pattern [4], which is an approach frequently used for computational modeling of other porous materials. Figure 3.2 shows an advanced approach that combines a beam model with the geometry computed from microstructure images.
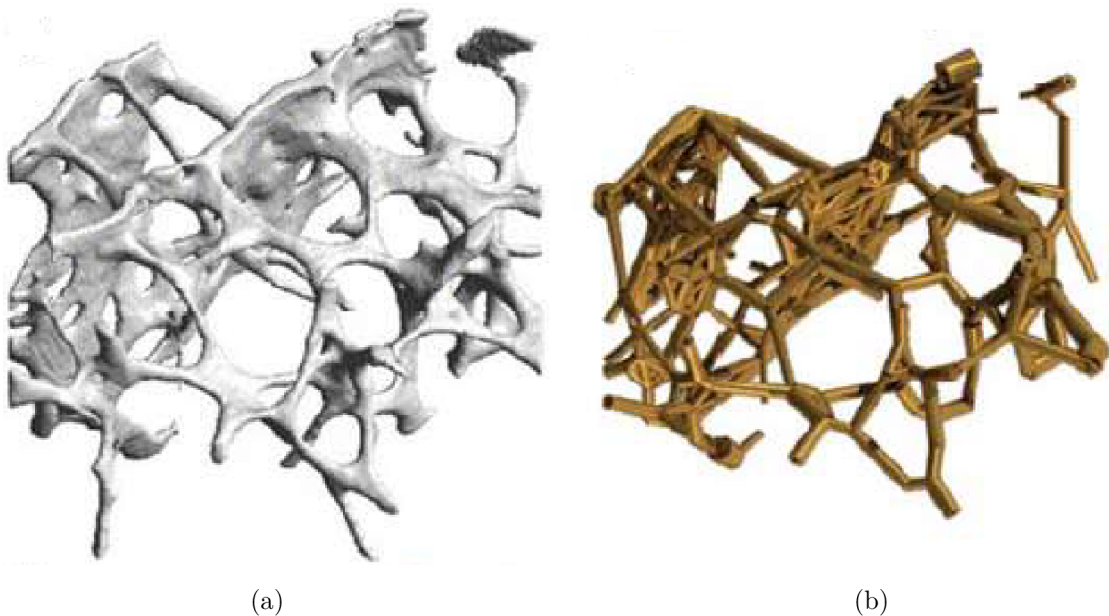

(a)   (b)

Figure 3.2: Comparison of the real bone sample (a) with the generated model based on the sample consisting exclusively of beams (b). Adapted from [4].

3.3.2. Beam and plate models

Dividing the spongy structure into plates and orthogonal rods as was illustrated in [3] takes into account two types of connections (see figure 3.3). The resemblance of the model is improved and the behavior of the geometry representation is closely related to the behavior of the spongy tissue. The idealization is based on the real structure and with the computational assistance, the real structure is basically decomposed into individual plates and rods 3.4. However, the theoretical model introduced in [4] decreases the volume and mass in comparison with the original structure, which implies that the deformation of the theoretical representation would deform on a larger scale.

3.3.3. Solid elements model

In the research of source [7] units called trabecular nodes are considered to be the basic unit of the spongy tissue model. It is accounted for the fact, that the structure of the tissue
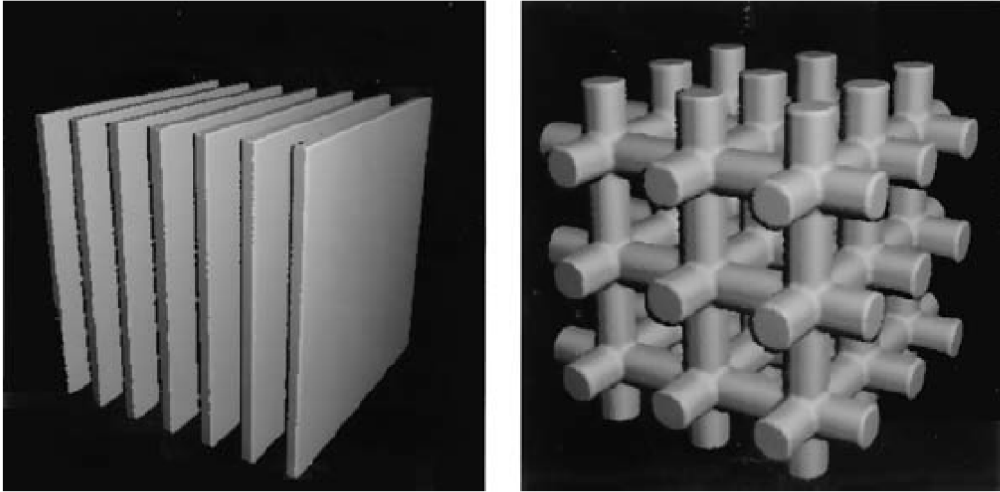
Figure 3.3: Left: plate units, right: rod units according to [3].

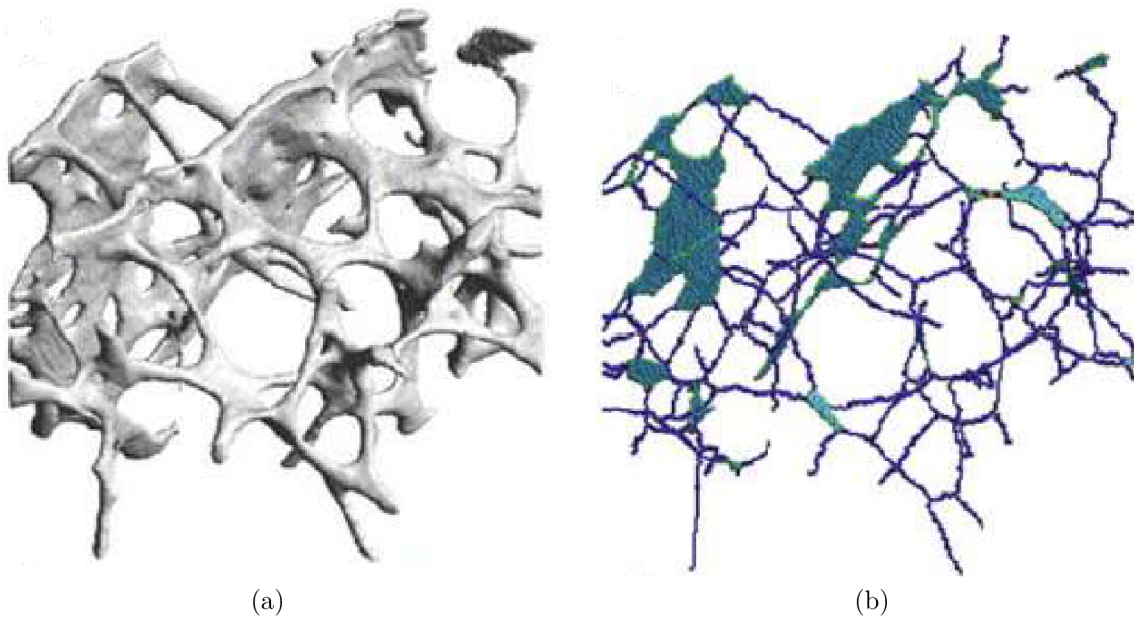(a)   (b)

Figure 3.4: Comparison of the real bone sample (a) with a generated model consisting of beams and plates (b). Adapted from [4].

(the inclination of the units and their dimensions) is not the same through all the bone. Therefore, the bone was divided into sections and models for each section with different inclination and node dimensions were created (see figure 3.5). The dimensions and the orientation of the solid elements were derived from the real structure by estimating the main direction of the load.

The main disadvantage of such model is found in the regularity of the representation, for example, the diameter of the connections is equal to a theoretical value and is not adjusted in dependence on location of the element.
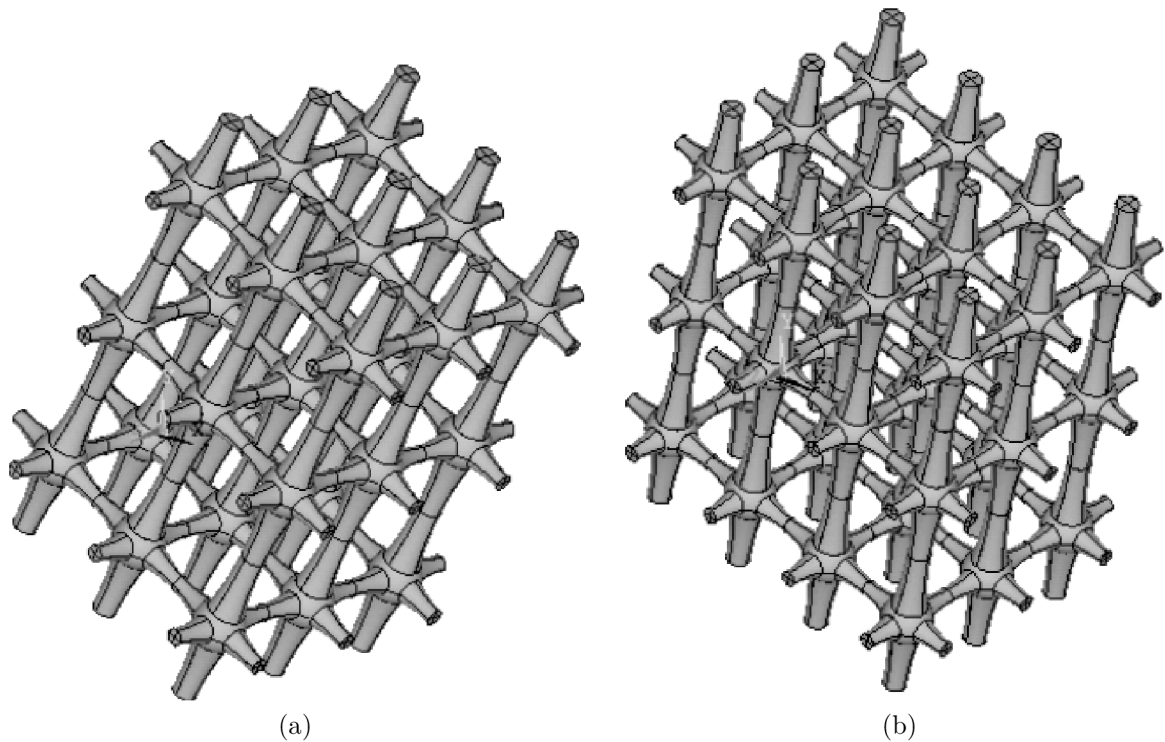
(a) (b)

Figure 3.5: The theoretical model of spongy tissue derived from an image of real tissue in the research [7]. (a) A theoretical model of Region 1 with inclination 30°, (b) a theoretical model of Region 2 with inclination 11°.

3.4. Modeling bone loss

Considering all the facts mentioned above, it is clear, that to model, generalize and make conclusions about real osteoporotic changes of the bone requires analysis of a great number of CT scans and a long-term individual approach to every subject, because the osteoporosis affects every single subject differently [14].

Nevertheless, the standard approach on how to model osteoporotic changes is experimental modeling [1], since the computational modeling is not reliable enough when it comes to linking the global level to the micro level bone tissue. The bone loss is simulated for example by demineralization and deproteinization of chosen animal long bones. There is one obvious disadvantage of the experimental approach: it is not viable *in vivo* since the sample needs to be collected.

Illustrating the changes on the models summarized above in chapter 3 is not only less complicated but also can be executed only by adjusting already generated theoretical models. Simulation of osteoporotic changes can be done by reducing the diameter of the rods (or generally connections) [1] in cancellous bone, respectively changing the thickness of the cortical layer. Another approach to modeling osteoporotic changes is by changing the strength (or other material property) of the material or by changing the architecture itself, which is more complicated though [4].

Applying geometry changes differs with the idealized geometry used. For example, the beam structure can be modified by deleting some of the beam connections [4], which will result in reducing the strength of the model.

3.5. Load distribution in the bones

Cortical bone is mainly subject to bending, whereas cancellous bone is adjusted to withstand compression [8] rather than tension [15]. The usual approach is to determine the load distribution during daily activities, the basic one is the standing position with no movement, then during physical activities such as running, walking, etc. For illustrating the stress distribution, the load distribution plot was enclosed, see figure 3.6.
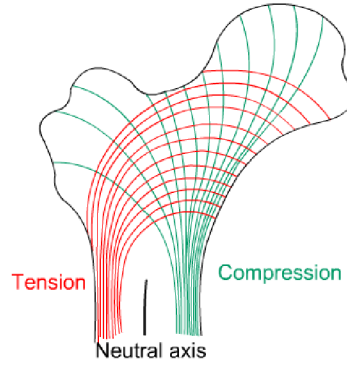

Figure 3.6: Stress lines connecting places with the same stress value [6].

According to the experimental methods of determining the load distribution [3], heterogeneity of the tissue must logically cause nonlinear stress distribution.

4. Bone FE modeling algorithm

It is important to mention the fact, that in theory, finite element analysis is the most accurate analysis so far [4] and it enables the subject-specific analysis. Furthermore, the algorithm is continuously perfected and the growing computational power of the devices enables the development of complicated problems. The application of the FEA to bone modeling is beneficial because it combines the advantages of accurate and detailed medical imaging with computational tools that provide precision. However, this method is still far too complex [14] to be incorporated to the health care practice, so other less accurate methods as Dual-energy X-ray are chosen to substitute FE methods.

The pre-analysis of the bone tissue, that is summarized in the list below has six steps, which result in creating the computational model of the bone. Those will also be used as a guideline to be followed in order to model the bone along with the right properties.

1. **CT scan** layer by layer resulting in a set of 2D images [8]

2. Extraction of the 3D model from CT scan files

3. Creation the surface representation (real or idealized)

4. Derivation of the solid body

5. Assignment of the material

6. Finite element analysis using computational tools

4.1. Preliminary steps

Before developing the actual modeling of the bone, it is necessary to derive the geometry from the real bone. This is usually done by using X-ray imaging. The most suitable scan is a Computed Tomography scan or CT scan in short. It is able to map bone morphology and density [8]. One of its advantages is, that using this non-invasive method, it is possible to obtain the data for picturing different layers of the bone [14].

The set of CT scans for the task of derivating the mechanical properties of the bone (see chapter 4.3 was taken from the Magnetic Resonance Research Facility, that has a complete collection of CT datasets called Visible Human for male and female bones available online [18].

However, for imaging the microstructure of different bone tissues, it is necessary to use micro-CT scans for deriving the geometry instead. Since the DICOM files [18] have a resolution (cubic voxel size) of 0,33 x 0,33 x 0,33 mm^3, they cannot be used for creating the microstructure computational model, since the difference between the bone and the void space in spongy bone is not distinguishable, however, the quality is sufficient for computing some of the whole-bone characteristics.

As for modeling the microstructure, especially the microstructure of a cancellous bone, another set of data: micro-CT scans of a human skull sample, provided by Ing. P. Marcián Ph.D. was used as a base data. The approach to the extraction of the geometry will be different than for the first set. This set has voxel dimensions 0,045 x 0,045 x 0,045 mm^3, which was more suitable for making conclusions about microstructure for it provides more

detailed insight. To illustrate the difference between those two sets, see the samples below 4.1.

Since the distribution of spongy tissue in the tibia is different from the tissue in the skull, caused by diverse normal loading conditions, linking the cortical and cancellous tissue is not possible and therefore, the morphologic types will be analyzed separately.

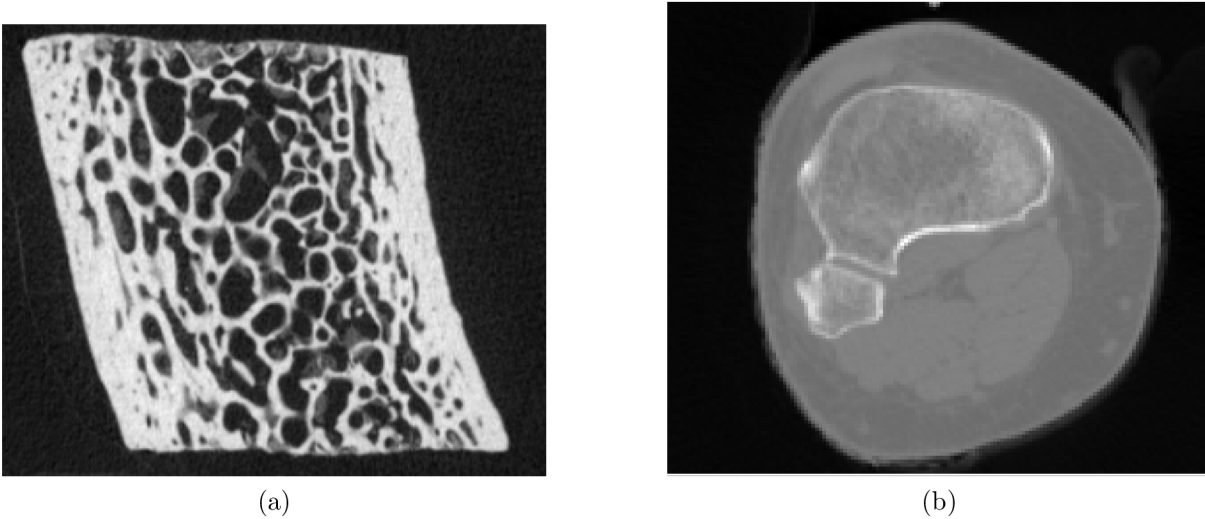(a)   (b)

Figure 4.1: Comparison of the difference between (a) a microCT image with resolution 0,045 mm - human skull sample and (b) a CT image of a resolution 1 mm - the female tibia [18].

4.2. Extraction of the structural mesh for property estimation

The first step in developing models of the bone is to obtain base data that will serve as a pattern to build on. Thanks to existing segmentation tools, the extraction of mesh data from the CT scans provided for analysis, is to use some of the segmentation tools for medical image computing. There is a great competition between research groups, therefore most of the software tools are available for free. However, it generally does not affect quality or functionality. National Institutes of Health and researchers [19] from universities all around the world are participating in the development together with sponsors that are making further development possible.

The tool chosen for analyzing the bone macrostructure (whole-bone properties) is a desktop application ITK-SNAP [19], due to the recommendation given by Dr. Eduardo Soudah. This software allows the user to easily extract the data necessary from the multislice scans, in this case, the available DICOM files from the set Visible Human Female [18]. The process of segmentation, distinguishing between tissue and void space [4], is semi-automatic, which means that human interaction is necessary to establish the conditions in the pre-segmentation phase. Following the segmentation stage [8], the tool renders the 3D geometrical representation of the subject sample.

The bone will be divided into two areas, as illustrated in figure 4.2 for more transparent analysis. The first section includes the epiphysis and metaphysis, where the cortical bone

16

is a thin shell surrounding the cancellous bone. The second section is located in the diaphysis, where the cortical bone can be illustrated as a hollow shaft [1] and will be the primary subject for subsequent analysis.
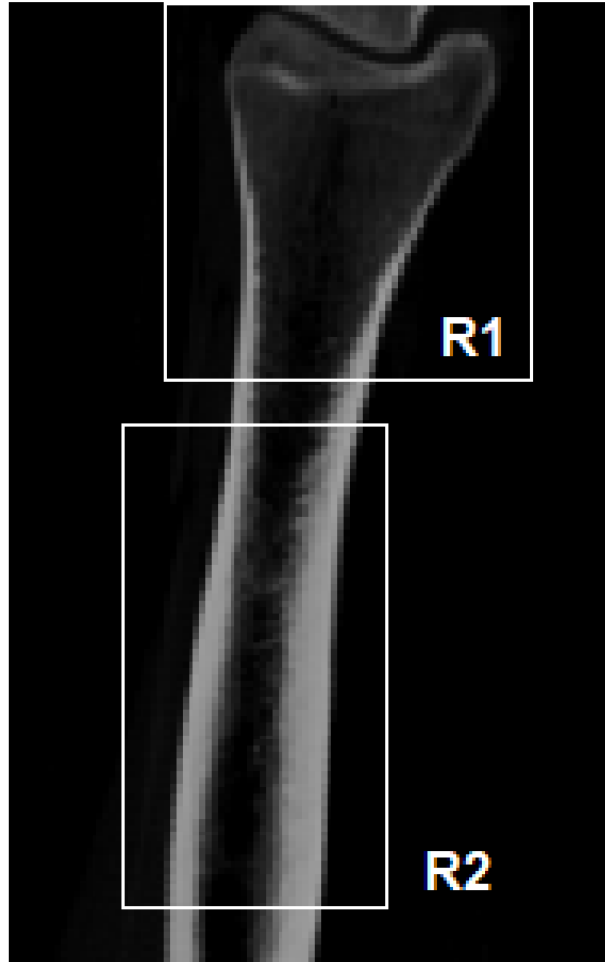

Figure 4.2: Allocation of the two separated regions in the tibia bone.
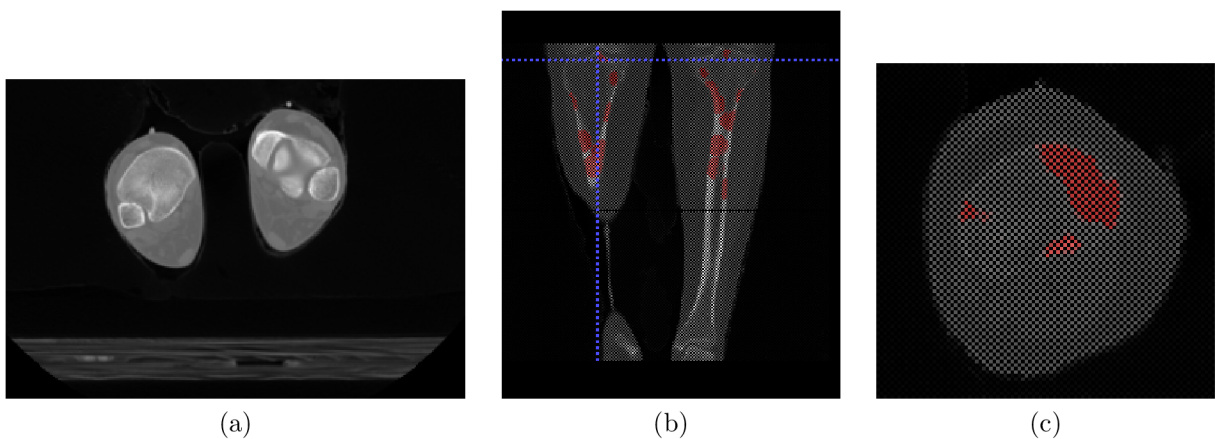

| (a) | (b) | (c) |

Figure 4.3: Segmentation process of the region R1 in ITK Snap [19], (a) original CT-scan image (b) the beginning of segmentation and (c) problematic region.

Though the algorithm introduced is useful, the tool has some minor issues when analyzing bones. The creation of a complete model of R1 requires two steps of segmentation [19] - the first one for creating the cortical bone representation, resulting in a hollow mesh, and another for generating the cancellous bone filling. This was done by adjusting the threshold. In the case of generating the model of the epiphysis, one additional manual step of adjusting the mesh was required, since some parts of connective tissue were not distinguished from the cortical bone at the initial stage, therefore some undesirable volume was attached to the model and it needed removing. This problem was caused by a low difference in density of this adjacent tissue, projected as a low difference in brightness on the CT images see figure 4.3c. The resulting ITK-SNAP mesh can be exported as a surface mesh .stl file, which can be simplified using functions offered in the ANSYS support system, Design Modeler.

The generated mesh of R1 (see figure 4.4) is used also for material property estimation and assignment in the next phase, the mesh of R2 is used for determining the displacement while loaded in chapter 4.5.1.
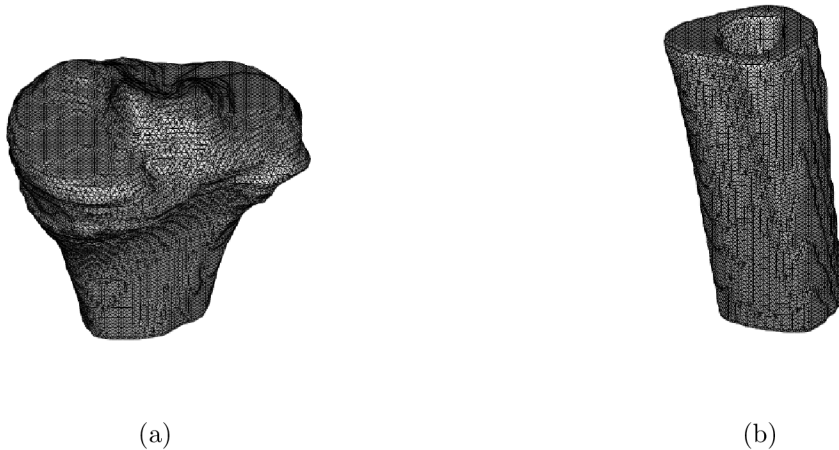

(a)   (b)

Figure 4.4: Generated models of (a) tibia joint and (b) tibia shaft [19].

4.3. Mechanical properties of the bone

The assignment of a single generally valid value for each mechanical property is not a viable method since the bones of every tested subject have shown slightly different values. According to Silva and Jepsen [11], even correcting the results by weight and height led to varying results for every patient. Therefore, the overall geometry will be based on a single set of CT data consisting of 356 images and the obtained values will be used as constants for the following analysis. This will probably induce some error (in comparison with theoretical values), which will be discussed further.

Nevertheless, the properties can differ even within the same bone, which is caused by the shape of the long bones [3]. The values of rigidity and strength differ comparing longitudinal and transverse cross-section: the elastic modulus of the cortical bone in a the longitudinal direction is equal to circa 17,4 GPa [3], whereas only 9,4 GPa in a transverse

direction. The standard mean value is established around 15 GPa up to 20 GPa [20]. The elastic modulus of the cancellous bone is up to thirty times lower [1, 14], which will be apparent in the next step of the analysis.

To describe the bone properties and establish the constitutive equations for analysis [3], three values of Young modulus E_{12}, E_{13}, and E_{23} among with three values of shear modulus G_{12}, G_{13} and G_{23} are usually chosen to represent the bone characteristics [2]. However, in this case, orthotropic material is idealized as isotropic, therefore the elastic modulus and shear modulus will be $E_{12} = E_{13} = E_{23}$ and $G_{12} = G_{13} = G_{23}$ respectively. Following the statement, that the ultimate tensile strength of bones is three times higher than ultimate shear strength [1], generally, the elastic modulus can be up to twenty times higher than the shear modulus [22]. To further illustrate the difference between the orthotropic and the isotropic model, tables 4.1 and 4.2 with values of elastic modulus of cortical and cancellous bone have been enclosed.

Table 4.1: Orthotropic vs isotropic model of cortical bone, adapted from sources [23, 3].

Parameter	Orthotropic [23]	Isotropic [3, 22]
E_{12}	18,155 GPa	15-20 GPa
E_{13}	6,983 GPa	15-20 GPa
E_{23}	6,983 GPa	15-20 GPa
G_{12}	4,69 GPa	< 4 GPa
G_{13}	5,61 GPa	< 4 GPa
G_{23}	7,68 GPa	< 4 GPa

Table 4.2: Orthotropic vs isotropic model of cancellous bone, adapted from [23] and [3].

Parameter	Orthotropic [23]	Isotropic [3]
E_{12}	2,029 GPa	7,8 GPa
E_{13}	2,029 GPa	7,8 GPa
E_{23}	3,195 GPa	7,8 GPa

Additionally, following the research by Stephen C. Cowin [3], we can preliminarily establish some of the load values, which were computed using analysis of the tibia of a 100kg person slowly climbing stairs. To determine the safety factors of the tibia, the range of tensile and compressive stresses had to be established at first. The tensile stress is, according to the same research, being ranged from 62,6 to 83,4 MPa and compressive stresses range from 72,6 to 90,4 MPa.

In the paper, they also mention, that during running, the force can climb up to three times the value of the body weight. That results in stress surpassing the yield strength but not exceeding the ultimate strength. Those results show, that during the daily activities, the bones are surprisingly exposed to stresses very close to the overall strength of the bone.

Table 4.3: Safety factors of the tibia [3] under tensile and compressive loading.

Parameter	Max stress	Average yield strength	Min safety factor
Tensile	83,4 MPa	128 MPa	1,53
Compressive	90,4 MPa	169 MPa	1,87

4.3.1. Estimated properties

Using the mesh computed from CT data in the first step, we can estimate mechanical properties of the bone given by the CT scan set, in this case, the Bonemat tool [17] was used. This software requires two files, a .vtk file obtained earlier and a .cdb file containing the FE model. The additional file with the configuration of the calculation (see figure 4.5) was created with the help of E. Soudah.

This configuration file assigns density and Poisson's ratio to every element according to their brightness in a CT image, giving a foundation for elastic modulus calculation. The density of both types of tissue is comparable [3] - 1914 kg m^{-3} for cortical and 1874 kg m^{-3} for cancellous bone. However, since the cancellous bone is porous, it appears as less bright material on the CT images.

```xml
<?xml version="1.0" encoding="UTF-8" standalone="yes" ?>
<CONFIGURATION Version="2">

  <CT_DENSITOMETRIC_CALIBRATION ROCalibrationCorrectionIsActive="true"
ROIntercept="-0.01185" ROSlope="0.0007034999999999999"/>

  <CORRECTION_OF_CALIBRATION IntervalsType="SINGLE">
    <CALIBRATION_SINGLE_INTERVAL a="0.079" b="0.877"/>
    <CALIBRATION_LIMITS RhoQCT1="0" RhoQCT2="0"/>
    <CALIBRATION_INTERVAL_1 a="0" b="1"/>
    <CALIBRATION_INTERVAL_2 a="0" b="1"/>
    <CALIBRATION_INTERVAL_3 a="0" b="1"/>
  </CORRECTION_OF_CALIBRATION>

  <DENSITY_ELASTICITY_RELATIONSHIP IntervalsType="SINGLE" MinElasticity="1e-06">
    <DENSITY_SINGLE_INTERVAL a="0" b="14664" c="1.49"/>
    <DENSITY_LIMITS RhoAsh1="0" RhoAsh2="10"/>
    <DENSITY_INTERVAL_1 a="0" b="14664" c="1.49"/>
    <DENSITY_INTERVAL_2 a="0" b="14664" c="1.49"/>
    <DENSITY_INTERVAL_3 a="0" b="14664" c="1.49"/>
  </DENSITY_ELASTICITY_RELATIONSHIP>

  <YOUNGMODULE CalculationModality="E" StepsNumber="4"/>

  <GROUPING GapValue="50"/>

  <ADVANCED DensitySelection="Mean" PoissonRatio="0.3" RhoUsage="rhoQCT"/>

</CONFIGURATION>
```

Figure 4.5: Configuration file establishing the calculation of Young's modulus [17].

The completion of the first step established above carried out the first results: information about Young's modulus of the elements. Figure 4.6 shows the analyzed mesh colored according to the elastic modulus of each segment. The values of the elastic modulus of this specific mesh were calculated to be within the interval from 360,349 MPa for minimal values at a cancellous bone up to 16,165 GPa at the cortical bone at the metaphysis. These values were calculated using Poisson's ratio equal to 0,3 through the whole structure and an approximation of the density - included in the configuration file.

The value of the elastic modulus of cortical bone corresponds with the value found in the source [3], mentioned above in this chapter. The difference between the theoretical and maximum calculated value is around 8% which can be considered negligible in this case.

The minimum value for cancellous bone is too low, the assignment was probably affected by the resolution of the images and therefore, the lowest value is affected by the pores. The theoretical value [3] of 7800 MPa will be used for further analysis instead.
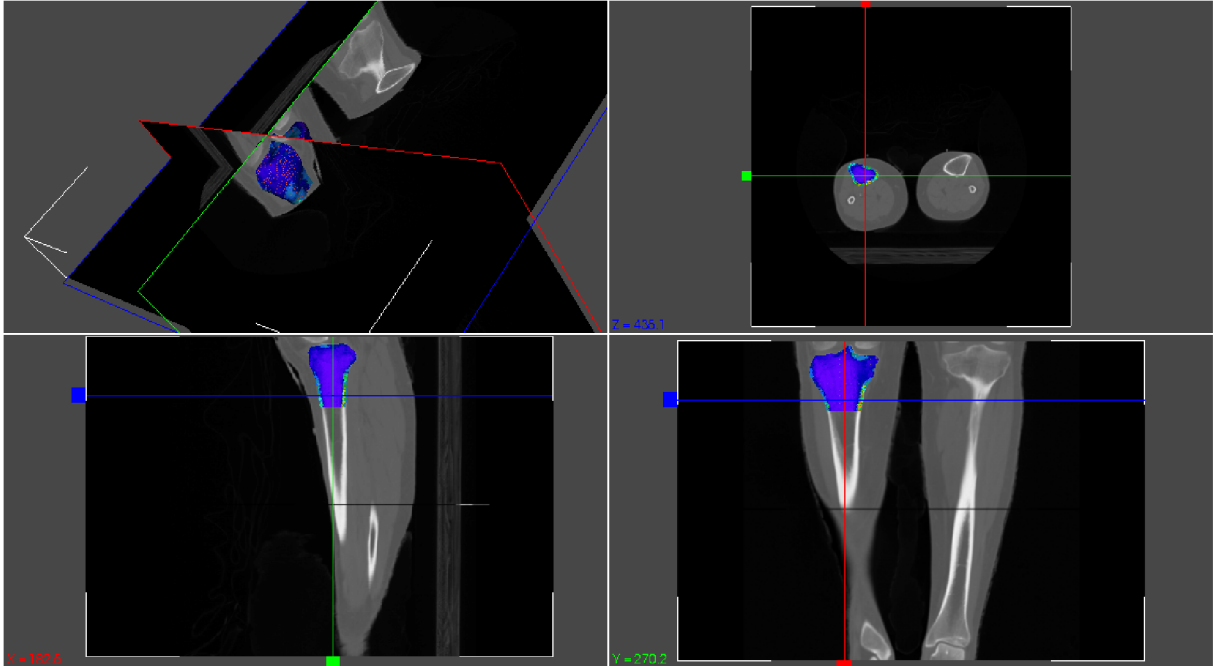

Figure 4.6: Orthoslice visualization of the distribution Young's modulus calculated using Bonemat tool [17].

4.4. Finite element analysis

The main part of the analysis is carried out in ANSYS Workbench [24]. It is obvious, that the correct establishment of the FE analysis is a crucial part of the whole process. The bone material was divided once again into three regions, as in figure 4.7. The first region is a solid compact cortical bone with no pores, the second region is a cancellous bone with rod and plate geometry and the last region can be described as a transition between the first two. The reason for this type of division is different geometrical representation - solid material [20], complex beam and rods structure [4] and solid material with spherical pores respectively. The modeling of the Region 3 will not be discussed any further since the sources focus mainly only on the first two types.

The assignment of the material was performed using values of density, elastic modulus and Poisson ratio from the chapter 4.3.1, with one exception, the Poisson ratio for the cancellous bone will be considered lower than the ratio of the cortical bone as in [16]. Before running the analysis itself, it is necessary to create loading and boundary conditions.
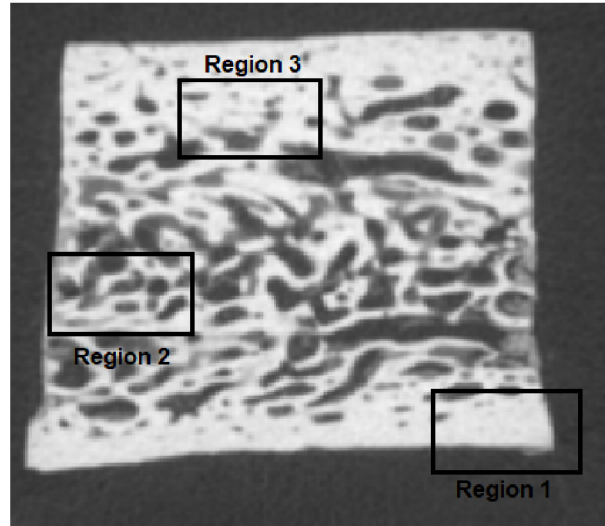
Figure 4.7: Definition of three regions, divided according to the geometry of tissue.

The following loading conditions are established: since compression is the most common type of loading [3], the mesh will also be analyzed under compressive loading. The value of loading force is established according to equation 4.1 expressing Newton's law. In this case, the load for one leg was established to the value of the half of the body weight [8]:

$$F = \frac{1}{2}\,mg = 0,5 \cdot 65 \cdot 9,81 = 318,83N, \tag{4.1}$$

where m is the mass of the subject and g is the gravitational acceleration. The value of the load is chosen for a normal standing position, the nominal stress (for mean diameter around 3 cm) will be roughly around 30% of the strength of the bone:

$$\sigma = \frac{F}{S} = \frac{4F}{\pi D^2} = 451kPa \tag{4.2}$$

where σ is stress in compression, F id loading force, D is mean diameter of the beam, resp. shaft. These two equations are a rough estimation of the loads acting on for femur bone neglecting the effect of muscles and other tissue. The load is transferred to the tibia, which is additionally supported by a calf bone. The static analysis of the bone system would require further analysis and is not a subject of this thesis, therefore, the loading force affecting the analyzed tibia will be left similar to the one calculated above.

Estimated properties and assumptions described in previous chapters affecting the analysis, are summarized in table 4.4 below.

Table 4.4: Summary of calculated values and assumptions according to former conclusions.

	Unit	Cortical bone	Cancellous bone	Reference
E	[GPa]	20	7.8	Chapter 4.3.1
ρ	[kg m^{-3}]	1914	1874	Figure 4.5
μ	[-]	0.3	0.25	Source [16]
Other		homogeneous, isotropic, linear elastic continuum		Chapter 3

4.5. ANSYS solution

According to the overview made in previous chapters, the models of microstructure are going to be prepared and analyzed using the toolset connected to ANSYS Workbench version 19.2 [24] and ImageJ visualization tools [21].

4.5.1. Analysis of cortical bone

At first, the cortical bone (Region 1 on figure 4.7) will be analyzed. Since the microstructure is approximated to be non-porous and the analysis of the small volume of this tissue does not require a complicated system of equations, a bit more complex analysis will be performed instead.

The aim is going to be to determine the difference in the deformation of simplified shaft geometry compared to the deformation of the shaft geometry from CT scans. The values for the idealized model were derived from the geometry extracted from the CT scans 4.2, the simplified structure is represented by a hollow shaft with the dimensions of outer diameter 28,3 mm and inner diameter 10,97 mm. Those dimensions were measured and averaged from the extracted model below 4.8 and it's cross-sections.
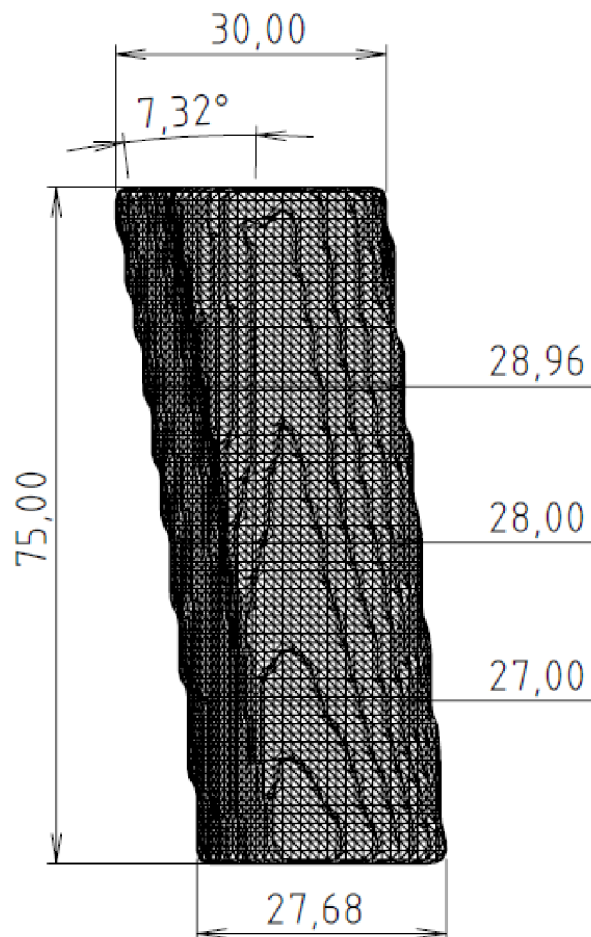

Figure 4.8: The dimensions of the extracted cortical bone shaft.

Apparently, the axis of the shaft is not exactly perpendicular to the horizontal plane, which will result in the bending stress affecting the bone while analyzing, implying, that

the bone is a subject to combined loading even in a normal upright standing position. The shaft geometry from CT scans was fixed on one end and compressed by a force with a magnitude defined above 4.9, which resulted in a deformation of 14.71 micrometers. Since the model was already pre-processed, the deformation caused by deflecting the force to the frontal area of the bone to simulate standing on toes was determined, see figure 4.10.
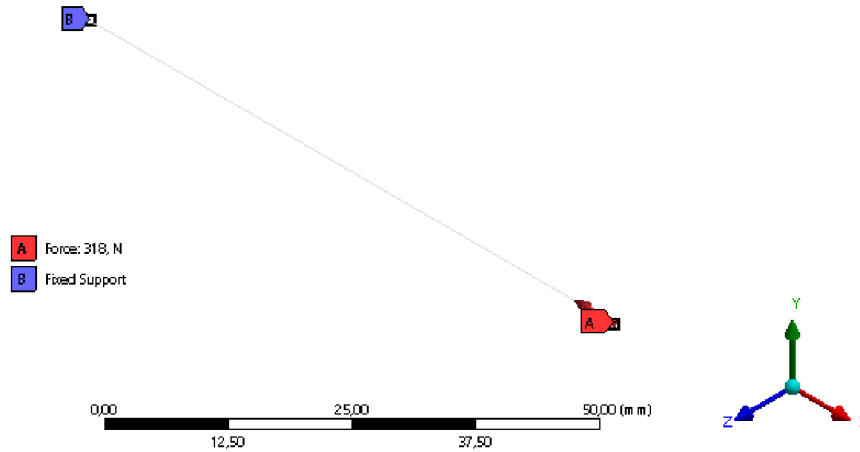

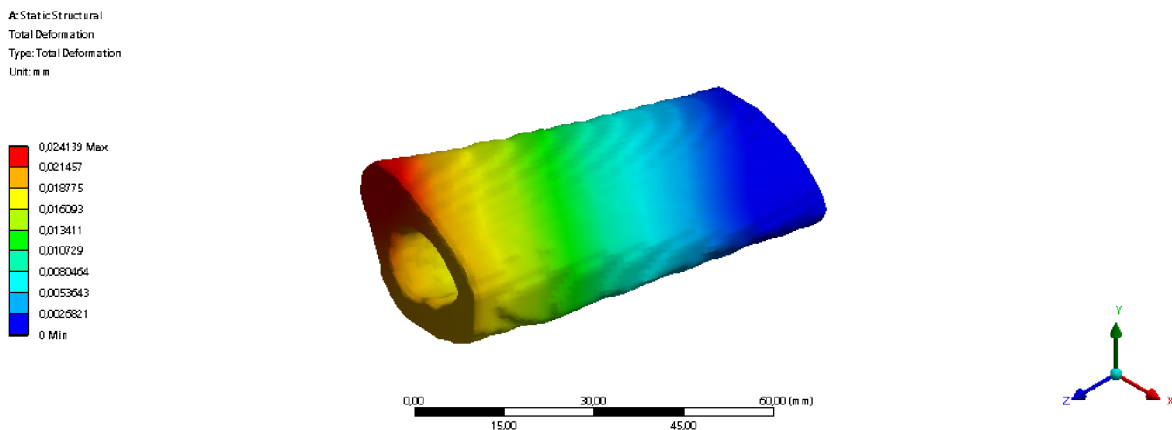Figure 4.9: The boundary conditions for the beam representation of the shaft.

Figure 4.10: The results of the force acting on the frontal part of the tibia.

As for the theoretical representation, two models of geometry were modeled to illustrate the difference between the deformation of the non-inclined and inclined shaft, see figure 4.11.

Before analyzing the more complex cancellous bone, the small volume of approximately 10 mm^3 of non-porous cortical tissue was analyzed, resulting in a calculation of displacement, which served as a reference value to the cancellous bone deformation. The cube 2.2 mm x 2.2 mm x 2.2 mm was compressed by a force of 12 N, which resulted in a 0.33 micrometers displacement on the y-axis.
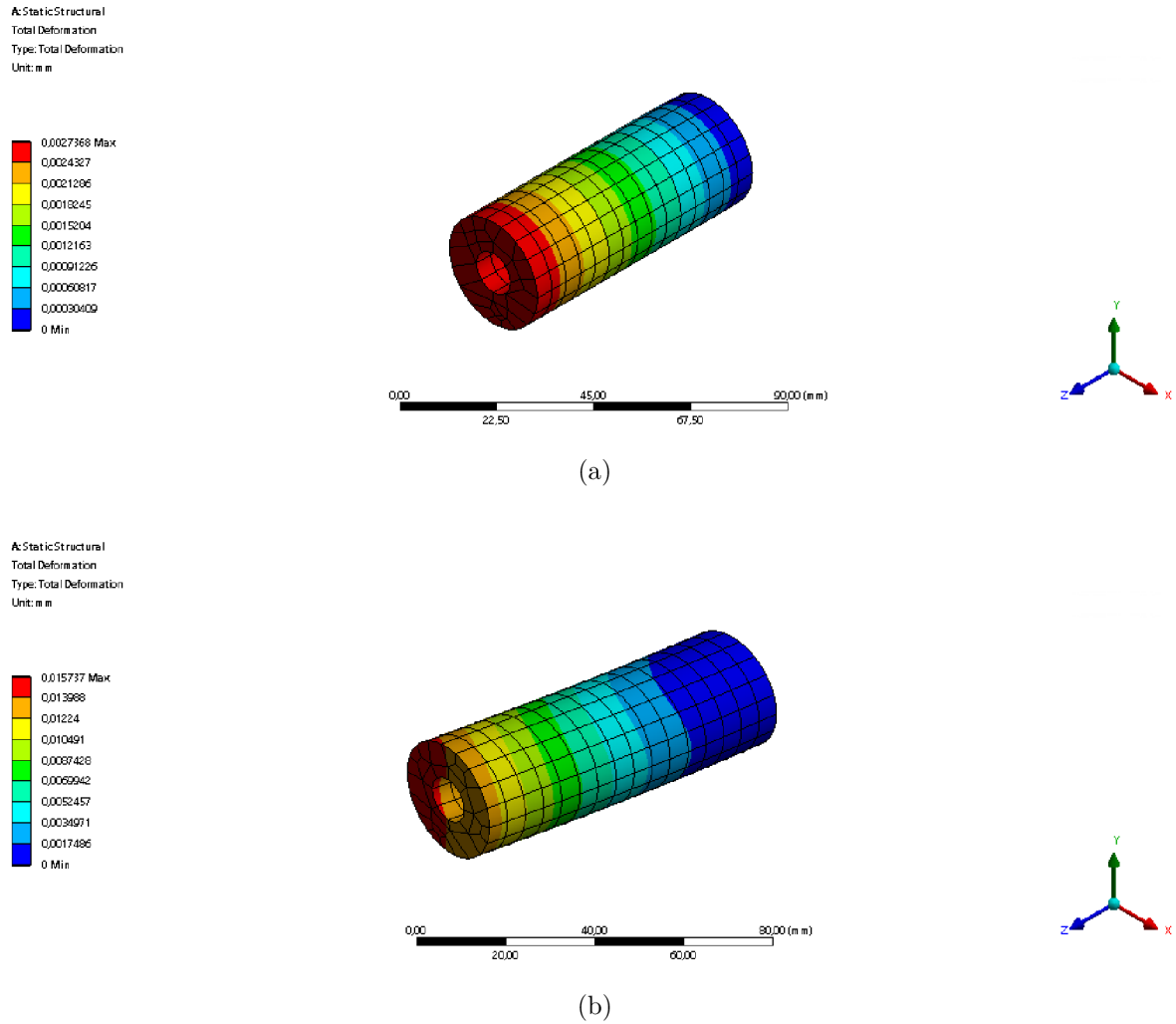
(a)

(b)

Figure 4.11: The impact of inclination of the shaft on the deformation (a) straight beam model (b) inclined beam model.
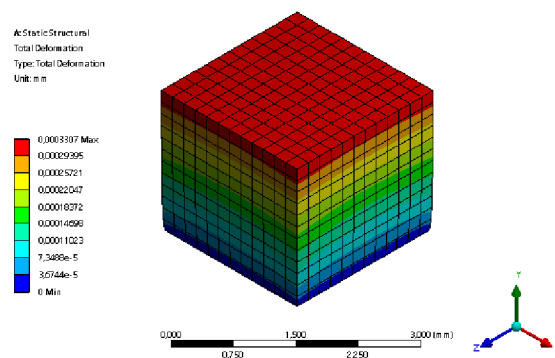

Figure 4.12: The reference calculation of displacement caused by compressing the cortical bone.

4.5.2. Models of the cancellous bone

The cancellous bone geometry represents a more complicated problem, which is apparent from chapter 3.3. The creation of the irregular geometry is based on μCT images of a

25

human skull, additionally, the dimensions of the substituting geometry are derived from these images. The visualization of sections of spongy tissue based on μCT images of the skull is performed using the functionalities of ImageJ, mainly a 3D Viewer tool. The tool allows the user not only to visualize the structure but also export it easily as a surface mesh in the .stl format.

Since the creation of the substitute models is complicated and as summarized in chapter 3.3 requires computational recognition of the substituting elements for sufficient visual representation, only a small volume of tissue will be analyzed.

Threshold value (boundary) for visualizing was set to 220 for perfect recognition of the tissue, see figure 4.13c. However, even the mesh of 50x50x50 pixels (50 pixels equals to approximately 2.2 millimeters) resulted in a body mesh composed of approximately 60 thousand triangular faces, which is not a problem for visualizing the structure, but it increases the time of the computation and requires more computational power to solve the problem. Sufficient representation is generated using a lower threshold value (200), with adjustment of the dimensions of the triangular faces, reducing the number of elements to approximately 15 thousand elements.

As mentioned above, the structural diversity of spongy tissue is very high, which was verified by visualizing different sectors of the tissue, see figure 4.13. The main visual difference can be observed when comparing section 4.13a and 4.13b. The samples originate from the same layer, however, the distance from the cortical layer varies.
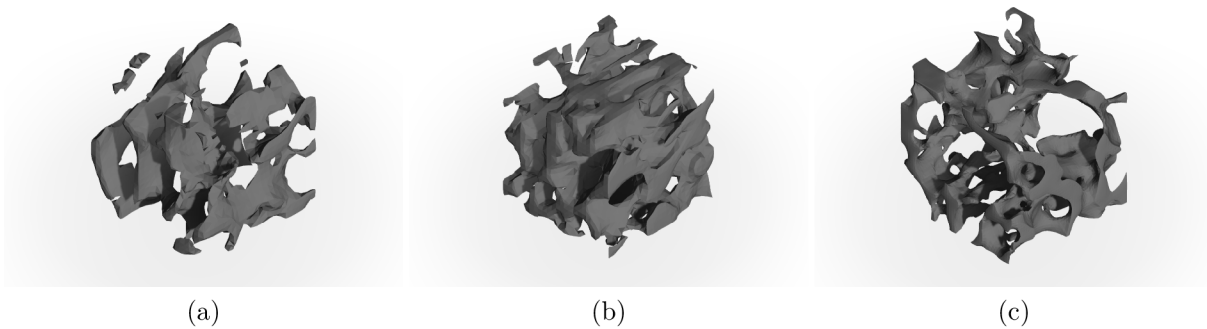

(a)   (b)   (c)

Figure 4.13: The samples of human spongy tissue generated from μCT images in ImageJ tool [21]

The models were generated specifically for the purpose of derivating the substitute geometry. The more complex analysis of those models is enabled only by the possibilities of the SpaceClaim tool built in the ANSYS software [24]. Together with the adjustment of the meshing options (the global settings were replaced by tetrahedral elements), the reference deformation under compression loading was established using the sample 4.13b.

Overall, the structure was deformed to 0.148 millimeters on average, however the remaining trabeculae in the upper left corner of the figure 4.14 below has shifted the scale because it has no supporting tissue and the force is acting on the nodes adjacent to its geometry. The overall validity of the generated mesh has been verified by calculating the force transferred to the fixed support at the bottom part - transferred force is equal to 11.9 N.

By analysis of the behavior of different spongy mesh, it is obvious, that stress concentration spots can be found even within the tissue, an example is illustrated (using the
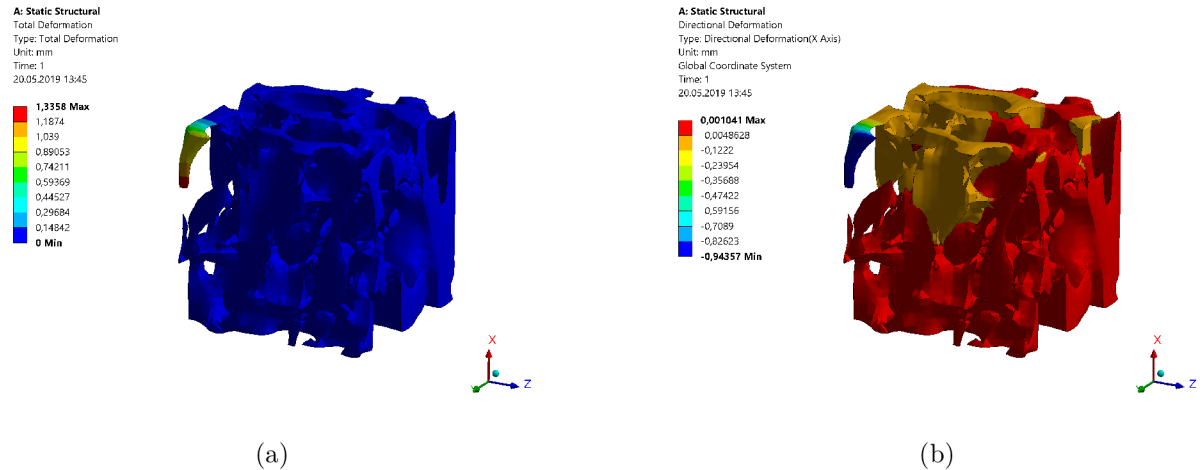
(a)   (b)

Figure 4.14: (a) total and (b) directional deformation of the spongy tissue under compression of 12 N.

von Mises equivalent stress) on figure 4.15, where the stress climbs up to ten times higher than the average stress inside the structure.
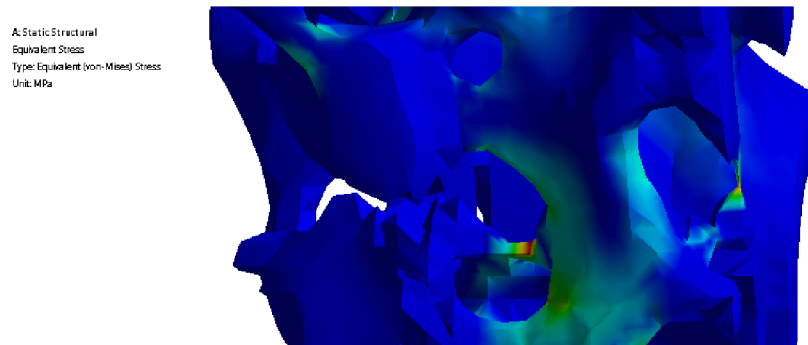

Figure 4.15: Stress concentration (calculated using von Mises theory), detailed view.

The same method for calculating another reference value of deformation as in the cortical bone model was used (a small volume of approximately 10 mm^3 was loaded by the same force of 12 N). The geometry was left nonporous, resulting in 0.68 micrometers displacement on the y-axis (the force is acting in the y-direction), which is double the displacement of cortical cube unit. The model is based only on the mechanical properties, due to the porosity of the tissue, the deformation of the real spongy is established to be a thousand times higher than in this basic case.

Establishment of the beam model

The complex model 4.13c was chosen as reference geometry for the beam models. The structure will be replaced by beams with A) circular and B) rectangular cross-section. For the creation of a substitute geometry, a file with coordinates of geometrical nodes identified in generated visualization of the real structure was created for importing directly into the Design Modeler tool for ANSYS. The beam system was based on those node points and a base frame, which was added to simulate the effects of adjacent structure and additionally to make the model more compact for analysis.

The main advantage of the Design Modeler tool is, that multiple cross-sections can be defined for a single project, which makes a comparison between these models easier. The cross-sections were based on data collected from micro-CT images and defined as follows:

1. The flattened plate-like beam with a rectangular cross-section with a height 0.2 mm and width 0.3 mm. The dimensions were measured using the ImageJ tool [21].

2. Rectangular cross-section with a height 0.3 mm and width 0.2 mm, which was added for evaluation of the impact of the orientation of the cross-section on the deformation.

3. Circular cross-section with a diameter of 0.28 mm. The diameter of the circular beam was established to 0.28 mm to match the cross-sectional areas of the two above.
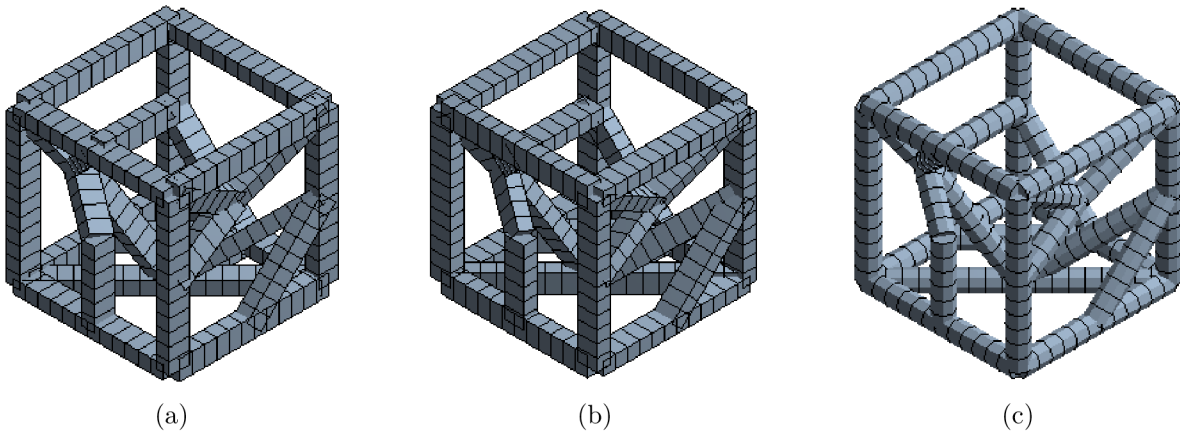

(a)   (b)   (c)

Figure 4.16: The beam representations of spongy tissue.

Establishment of the plate model

By analyzing the micro-CT scans of the skull visualized on figure 4.13, it is apparent, that the connections are not the only elements present in the structure. The plates are easily recognized near the center of the analyzed specimen, figure 4.13a. The theoretical representation was based on plate geometry of a plate thickness equal to 0.23 mm, identified and measured from the real structure. The plates were further simplified as parallel with the loading direction.

Comparison of the generated models

Since the material is defined as an elastic continuum (the behavior in tension and compression loading can be described by Hooke's law), the comparison of the models can be made using relative displacement according to equation 4.3.

$$\epsilon = \frac{\Delta L}{L_0} \tag{4.3}$$
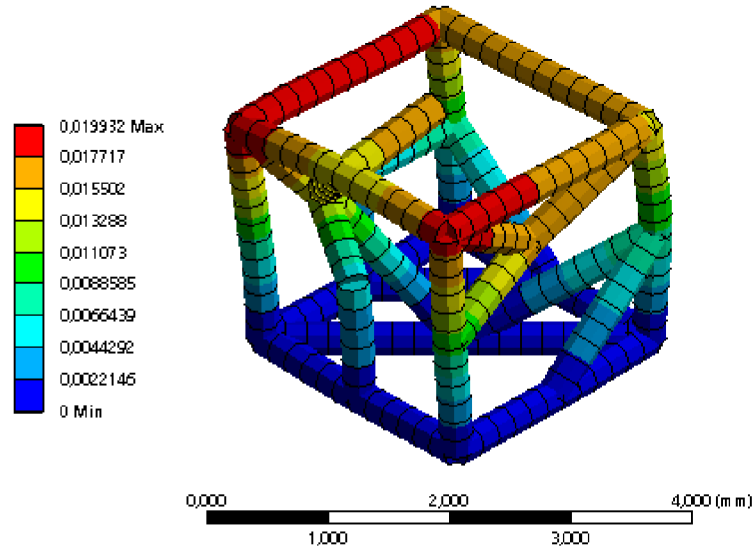
Figure 4.17: The analysis of the beam system with a circular cross-section, which was based on the cancellous geometry.
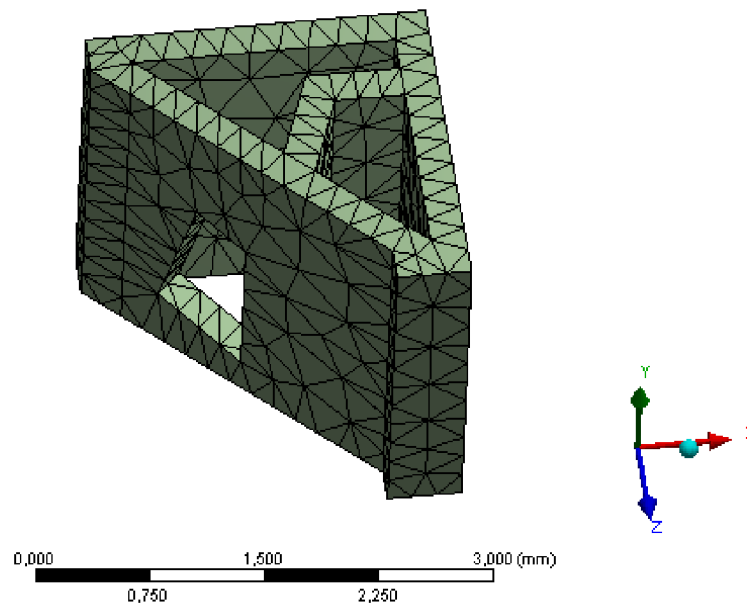
Figure 4.18: Straight plate model based on observation of the spongy tissue in the human skull, geometry created in Solidworks 2018 software [25].

The comparison of the idealized shaft geometry with the geometry derived from CT scans using the deformation is summarized in table 4.5 below.

The results for the deformation of cortical bone modeled as an inclined beam correspond with the deformation of the real structure differing only by 1 micrometer in total and 2 micrometers in directional deformation. The analysis implies, that the idealization by straight beam results in the deformation equal to one-third of the deformation of the

Table 4.5: Deformation of the tibia shaft (cortical bone only). U stands for total deformation, u_z for directional deformation in the z-axis and ϵ is relative displacement.

Geometry	U [μm]	u$_z$ [μm]	ϵ[-]
Simple shaft	2.74	2.74	$3.65 \cdot 10^{-5}$
Inclined shaft	15.74	8.86	$1.15 \cdot 10^{-4}$
Standing position	14.71	10.88	$1.45 \cdot 10^{-4}$
Frontal area load	24.14	14.1	$1.88 \cdot 10^{-4}$

computed model. When standing on toes, the directional deformation increases only by 4 micrometers, however the total deformation increases by 10 micrometers, which confirms the theory, that even though the compression loading is the main type of loading influencing the bone during daily activities, other types of loading deform the structure on a greater scale.

Table 4.6: Deformation of the spongy tissue from a human skull, arranged according to the order they are established.

Geometry	U [μm]	u$_z$ [μm]	ϵ[-]
Computed model	148.42	122.2	$54 \cdot 10^{-3}$
Simple cube	0.68	0.68	$0.3 \cdot 10^{-3}$
Circular beam	19.93	14.94	$6.63 \cdot 10^{-3}$
Rectangular beam 1	20.39	15.07	$6.7 \cdot 10^{-3}$
Rectangular beam 2	22.16	15.64	$6.95 \cdot 10^{-3}$
Plate model	2.39	2.32	$1.03 \cdot 10^{-3}$

The provided results differ in the order of magnitude. The idealized models react to the same loading conditions on a lower scale, caused the rigidity induced by simplifying the structure. Even though concentration factors were induced to the idealized structures, the deformation is up to seventy times lower.

Some similarities between the real geometry representation and the theoretical model can be found, for example, the stress concentration similarity has been reached in the plate model, the substitute geometry shows the maximum equivalent stress being 10 times higher than the average stress within the model.

5. Osteoporotic changes in the bone

The osteoporotic changes will be simulated on the theoretical models in two different ways. The first method is geometrical transformation - thinning the cortical layer and decreasing the dimensions of beams in spongy bone. This will affect the displacement of the geometry. A different approach is to manipulate the tissue properties - in this case, the elastic modulus.

Applying the geometry transformation to cortical bone model by diminishing the width of the cortical layer by 0.074 mm (according to [26]) resulted in increased displacement by 0.0145 micrometers in the straight shaft model, which is only by 0.02% more than in the non-affected straight shaft model, however, the representation has not proven as reliable as the inclined shaft model, which total deformation increased by 0.062 micrometers and the directional deformation in the direction of acting force by 0.028 micrometers - $4 \cdot 10^{-7}$ of relative displacement change. However small these numbers can seem, the deformation increases by decimal places in another type of loading than standing [16].

The geometry adjustment of the cancellous representation is a bit more complex. The simulation of osteoporotic changes for this type of tissue was performed by decreasing the beam dimensions, which were adjusted to 0.273 mm for circular cross-section (decreased by 7 micrometers) and to 0.3 mm x 0.19 mm for the rectangular beam. The simulation of the bone loss was completed by removing two beams from the system.

The thickness of plates was adjusted similar was to the beam model to a value 0,219 mm, additionally, an irregular hole was added as a simulation of increasing porosity during the prevailing resorption of the tissue. The results of these changes are summarized in table 5.1 below.

Table 5.1: Deformation of the idealized geometry affected by geometric osteoporotic changes.

Geometry	U[μm]	u_z [μm]	Δu_z [μm]
Circular beam	359.77	312.92	297.98
Rectangular beam 1	410.76	339.47	324.4
Rectangular beam 2	411.59	326.56	310.92
Plate model	3.19	3.11	0.79

Table 5.2: Deformation of the geometry with changed mechanical properties to simulate osteoporotic changes.

Geometry	U [μm]	u_z [μm]	Δu_z [μm]
Simple cube	1.02	1.02	0.34
Circular beam	29.89	22.48	7.41
Rectangular beam 1	30.58	22.61	15.91
Rectangular beam 2	33.24	23.45	16.5
Plate model	3.59	3.49	1.17

The adjustment of elastic modulus was performed using the findings of the source [27], that derives the decrease in elastic modulus of the mouse tissue from an experiment. The

result is estimated to be equal to 30% of the non-affected elastic modulus. The values of the idealized representations have therefore been diminished to two-thirds of the original elastic modulus 7.8 GPa, the substituting Young modulus therefore equal to 5.2 GPa.

6. Conclusion

The methods of idealizing bone tissue are always based on structural assumptions leading to simplifications and negligence of the bone tissue and its properties for the cost of the credibility of the models. The theoretical part of this thesis summarized the variety of bone modeling methods, which is broadened with growing computational power.

The initial part of the computational part was focused on determining Young's modulus from CT scans of the female tibia. Even though the resolution of those scans was not found sufficient for determining the elastic modulus of the cancellous tissue due to poor quality scans, the computed value of elastic modulus of cortical tissue computed using the freeware ITK Snap lays within the interval found in the literature (15 to 20 GPa) [3].

The results of displacement while replacing the geometry of the shaft by a beam geometry were similar even though the shape differed especially in the cortical thickness in the front part of the bone, where the cortical layer is wider as a reaction to loading conditions during daily activities.

As for the microstructure, the displacement under compression of the small volume was chosen as a property of interest. This value is based on the assumption, that the bone deforms according to Hooke's law (linearly). If further research were to be conducted, the non-linear behavior should be implemented instead.

Importing the geometrical representations of the real spongy tissue to ANSYS Workbench 19.2 has proven a lengthy process since the models are composed of 15 thousand faces even though the generated volume is only 11.4 mm^3, confirming the fact, that the mass of the tissue is small compared to the surface. The solution in this tool is not optimal for the spongy tissue, the usage of ANSYS Classic tool was suggested instead (for further study and more precise results), since the analysis of porous materials is used more frequently and the results are validated.

Finally, the small volume geometry replacement was not found credible, since the deformation of the structure derived from the CT scans has resulted in a displacement up to seventy times higher compared to the idealized models. The connections between the beams in the beam model were left default, which could be further improved by adding a smooth transition, resulting in improved reliability and credibility of the model. Furthermore, the substitute geometry dimensions were constant, which could have affected the analysis further. The problem of a wide variety of basic unit could be resolved by adding a computer recognition of those units (beams and plates) together with their dimensions, which could serve as an inspiration for new research.

The plate model has proven the least reliable for determining the displacement of the trabecular tissue under defined loading conditions, however, the simulation of osteoporotic changes by both geometrical transformation and transformation of mechanical properties have shown similar results.

The deformation of the beam models was established to be eight times lower than the deformation of the real tissue, however the deformation increased after exposing the geometry to the effects of osteoporosis. The displacement increased up to a value two times higher than the displacement of the real geometry, which was not subjected to osteoporotic changes, and twenty times higher than in the initial theoretical model. The conclusion from the modeling of the geometry is, since the change in elastic modulus did not have such an impact, that such a porous geometry is highly sensitive to any change in the supporting structure.

The geometrical representations of the osteoporotic structure An additional model of the transitional bone (established as R3 on figure 4.7) is proposed to be added to the comparison of the idealized cancellous bone representation, which could be generated by removing the full material by spherical geometry. The mechanical properties of this transitional region are proposed to be defined between values of cortical and cancellous bone. The visualization tools for trabecular bone, e. g. ImageJ [21] already offers the possibility to fit spheres into the volume, even though the purpose is not to create a 3D representation.

Bibliography

[1] VOSYNEK, P.: *Analýza odezvových veličin kostní tkáně při mechanickém zatěžování.* [Disertační práce.] Vysoké učení technické v Brně, Fakulta strojního inženýrství, 2015. 98 s. Vedoucí dizertační práce Ing. Tomáš Návrat, Ph.D.

[2] NEČAS, D.: *Deformačně napěťová analýza stehenní kosti s využitím dat z počítačové tomografie.* [Diplomová práce.] Brno: Vysoké učení technické v Brně, Fakulta strojního inženýrství, 2012. 96 s. Vedoucí diplomové práce Ing. Petr Vosynek.

[3] COWIN, S. C.: *Bone mechanics handbook. 2nd ed.* Boca Raton, FL: CRC Press, 2001. ISBN 0849391172.

[4] DE, S., GUILAK, F. and MOFRAD, M. R. K.: *Computational Modeling in Biomechanics.* New York: Springer, 2010. 579 p. ISBN 978-90-481-3574-5.

[5] VAUGHAN, T. J. and McNAMARA, L. M.: Multiscale modeling in biomechanics: *Multiscale modelling of bone: Understandung tissue mechanics and cell mechanobiology.* 18th Congress of the European Society of Biomechanics, 2012.

[6] CAPES, J. and McCLOSKEY, C.: Biomaterials and Biomedical Materials: *Structure of Bone and Implant Materials.* University of Cambridge, October 2006. [cit. 2019-04-02]. Dostupné z: https://www.doitpoms.ac.uk/tlplib/bones/index.php

[7] LASTOVKINA, Y. N. and KOLMAKOVA, T. V.: Computer modelling of the microstructure of the trabecular bone fragments for the study of stress-strain state. In *J. Phys.: Conf. Ser.* 769 012020, 2016.

[8] FRANCIS, A. and KUMAR, V.: Computational Modelling of Human Femur using CT Data for Finite Element Analysis. In *IJERT.* August 2012, vol. 1, no. 6. ISSN 2278-0181.

[9] KINI, U. and NANDEESH, B. N.: Physiology of Bone Formation, Remodeling and Metabolism. In *Radionuclide and Hybrid Bone Imaging.* Berlin, Springer, 2012. p. 29-57. ISBN 978-3-642-02400-9.

[10] BLACK, C. R. M, et al.: Bone Tissue Engineering. In *Curr Mol Bio Rep.* Berlin, Springer, 2015, vol. 1, no. 3, p. 132-140. ISSN 2198-6428.

[11] SILVA, Matthew J.: *Skeletal aging and osteoporosis: biomechanics and mechanobiology.* New York: Springer, 2013. Studies in mechanobiology, tissue engineering, and biomaterials, 5. ISBN 3642180531.

[12] TAGHIZADEH, E., et al.: Fast Prediction of Femoral Biomechanics Using Supervised Machine Learning and Statistical Shape Modeling. In *Computational Biomechanics for Medicine* Springer, 2016, p. 107-116. ISBN 978-3-319-28329-6.

[13] FUNG, Y. C.: Bone and Cartilage. In *Biomechanics: mechanical properties of living tissues.* 2nd ed. New York: Springer-Verlag, 1993, p. 500-544. ISBN 3540979476.

[14] JOLDES, Grand R. et al.: Computational biomechanics for medicine: imaging, modeling and computing. New York, NY: Springer Science+Business Media, 2016. ISBN 978-3-319-28327-2.

[15] OSTERHOFF, G., et al.: Bone mechanical properties and changes with osteoporosis. *Injury.*, June 2016, vol. 47, no. 2, p. 11-20. ISSN 0020-1383.

[16] PAWLIKOWSKI, M., et al.: Stress–strain characteristic of human trabecular bone based on depth sensing indentation measurements. *Biocybernetics and Biomedical Engineering*, February 2017, vol. 37, p. 272-280. ISSN 0208-5216.

[17] TADDEI F., et al.: The material mapping strategy influences the accuracy of CT-based finite element models of bones: an evaluation against experimental measurements. it Med Eng Phys. November 2007; vol. 29(9), p. 973-9. ISSN 1350-4533.

[18] ACKERMAN, M. J.: The Visible Human Project. *Proceedings of the IEEE*, March 1998, vol. 86, no. 3, p.504-511. ISSN 0018-9219.

[19] YUSHKEVICH, P. A., et. al.: User-guided 3D active contour segmentation of anatomical structures: Significantly improved efficiency and reliability. *Neuroimage.* July 2006; vol 31(3), p. 1116-1128. ISSN 1053-8119.

[20] FRAME, J. C., WHEEL, M. A. and RICHES, P. E.: A numerical investigation and experimental verification of size effects in loaded bovine cortical bone. *Int J Numer Method Biomed Eng.* May 2017; vol 34(1), ISSN 2040-7947.

[21] DOUBE, M., et. al.: BoneJ: Free and extensible bone image analysis in ImageJ *Bone.* September 2010; vol 47 (6), p. 1076-1079, ISSN 8756-3282.

[22] WIRTZ, D. Ch., et. al.: Critical evaluation of known bone material properties to realize anisotropic FE-simulation of the proximal femur *Journal of Biomechanics.* March 2000; vol 33, p. 1325-1330. ISSN 0021-9290.

[23] YOUSIF, A. E., AZIZ, M. Y.: Biomechanical Analysis of the human femur bone during normal walking and standing up. *IOSR Journal of Engineering.* August 2012; vol. 2, no. 8, p. 13-19, ISSN 2250-3021.

[24] ANSYS® Academic Research Mechanical, Release 19.2, Help System, Coupled Field Analysis Guide, ANSYS, Inc.

[25] DASSAU SYSTEMES SOLIDWORKS: Solidworks Web Help [online] March 2010. Available at: https://help.solidworks.com/

[26] SADAT-ALI, M., et. al.: Tibial cortical thickness: A dependable tool for assessing osteoporosis in the absence of dual energy X-ray absorptiopmetry. *Int J Appl Basic Med Res.* 2015; vol 5(1), p. 21–24. DOI:10.4103/2229-516X.149228.

[27] CHON, C.-S., et. al.: Elastic Modulus of Osteoporotic Mouse Femur Based on Femoral Head Compression Test. *Appl Bionics Biomech.* 2017; DOI:10.1155/2017/7201769.